**Biophysical Journal, Volume *111***

## Supplemental Information

# Single-Molecule Imaging of $Na_v1.6$ on the Surface of Hippocampal Neurons Reveals Somatic Nanoclusters

**Elizabeth J. Akin, Laura Solé, Ben Johnson, Mohamed el Beheiry, Jean-Baptiste Masson, Diego Krapf, and Michael M. Tamkun**

## MATERIALS AND METHODS

### Actin PALM imaging

We simultaneously imaged actin with super-resolution by PALM and cell surface $Na_v1.6$-BAD labeled with CF640R. Neurons were transfected with $Na_v1.6$-BAD and photoactivatable-GFP-actin (paGFP-actin). Before TIRF-based imaging, $Na_v1.6$-BAD was labeled with SA-CF640R and the cells then sequentially fixed with 0.3% glutaraldehyde for 1 min and 2% glutaraldehyde for 10 min prior to an incubation with 0.1% $NaBH_4$ for 7 min to reduce the fluorescence background. The channels were first imaged to determine their surface distribution. PALM was then used to localize single actin molecules in close proximity to the plasma membrane, i.e. within the TIRF excitation field. paGFP was converted from its non-fluorescent state to the fluorescent state using the 405nm-laser and the activated molecules were visualized and subsequently photobleached using high intensity 488 nm laser light. All the laser lines were maintained in TIRF to photoconvert and image only at the basal surface. Super-resolution images of actin localization were reconstructed using the ImageJ plugin ThunderSTORM (1). TIRF images of surface $Na_v1.6$-BAD (non-super-resolution) were overlaid on the super-resolution image of actin. TetraSpeck beads were used as fiduciary markers to correct for drift.

### Actin depolymerization

Neurons were transfected with $Na_v1.6$-BAD and Ruby-Lifeact (gift from Dr. James Bamburg, Colorado State University). The surface distribution of $Na_v1.6$-BAD was again visualized with SA-CF640R. Transfected neurons were imaged in TIRF at one Hz for ~10 min to establish a baseline. SwinholideA (200 nM) was then added to the bath and actin depolymerization

monitored via Ruby-Lifeact. Neurons were imaged every 1 min for an additional hour to determine the effect of actin depolymerization on $Na_v1.6$-BAD distribution.

## RESULTS

### Distribution of $Na_v1.6$ surface puncta intensities in neurons and glia

$Na_v1.6$-BAD was transfected into neuronal cultures and the surface-labeled channels were imaged using TIRF microscopy. The measurement of $Na_v1.6$-BAD surface puncta fluorescence intensities in neurons and glia allowed for a comparison of the surface distribution between these cell types. The distribution of surface puncta intensities illustrated in Fig. S1 shows high intensity values, i.e. $Na_v1.6$ nanoclusters, in neurons that are absent from glia. These results suggest that nanoclustering of $Na_v1.6$ is cell-type specific.

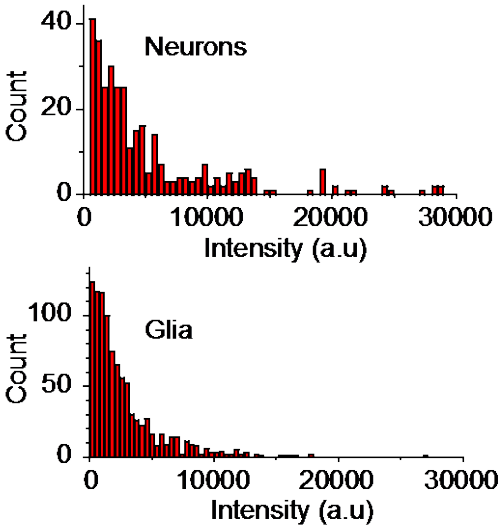


**SUPPLEMENTARY FIGURE 1** Histogram of puncta intensities for both neurons and glia. Cell surface $Na_v1.6$ was labeled with SA-CF640R and the fluorescence intensity of individual surface puncta, representing both single channels and channel aggregates, was measured. Summed data from three neurons and three glial cells are presented.

### $Na_v1.6$ nanoclusters are actin independent

Since the localization mechanism of somatic $Na_v1.6$ is not due to ankyrin-binding, we hypothesized that other cytoskeletal components may be involved. Indeed, actin is involved in the localization of $K_v2.1$ to large, micron size clusters on the soma of some neurons (2) as well as influencing the diffusion of a number of membrane

proteins. Thus we wanted to determine whether $Na_v1.6$ nanoclusters are also stabilized by cortical actin. Actin is present throughout nearly the entire neuron, while $Na_v1.6$ nanoclusters represent a very small fraction of the neuronal membrane. In order to determine whether there is any distinct actin organization present around the $Na_v1.6$ nanoclusters we used super-resolution microscopy such that actin molecules could be resolved below the diffraction limit. For this, we used photoactivation localization microscopy (PALM) of photoactivatable-GPF actin (paGFP-actin). Neurons were co-transfected with $Na_v1.6$-BAD and paGFP-actin and the $Na_v1.6$ surface distribution was visualized with SA-CF640. The 405-nm laser was used to activate low numbers of the paGFP-actin molecules, and the 488-nm laser was used to visualize and photobleach activated particles. Activated fluorophores were fit with a Gaussian distribution to localize particles. The localizations from each frame were reconstructed into a super-resolution image of the cortical actin for a DIV11 rat hippocampal neuron.

The image acquired using standard TIRF microscopy is displayed on the left side of Fig. S2A and the super-resolution reconstruction on the right. Fig. S2B shows an enlargement of the white box in Fig. S2A to demonstrate the relative distribution of $Na_v1.6$ and actin. Again, the image obtained by standard TIRF microscopy shows little fine structure (top panel), while PALM-based super-resolution clarifies the location of the actin (middle panel). Somatic $Na_v1.6$ channel nanoclusters localize to membrane regions distinct from, but often adjacent to, cortical actin structures present in the TIRF field (yellow arrows, middle and bottom panels). This spatial relationship is further demonstrated by the line scan in Fig. S2C, which is derived from the normalized fluorescence intensity of actin and surface-labeled $Na_v1.6$-BAD along the dotted line in Fig. S2A. While the cortical actin filaments did not localize with the $Na_v1.6$ nanoclusters the two were often in close proximity.

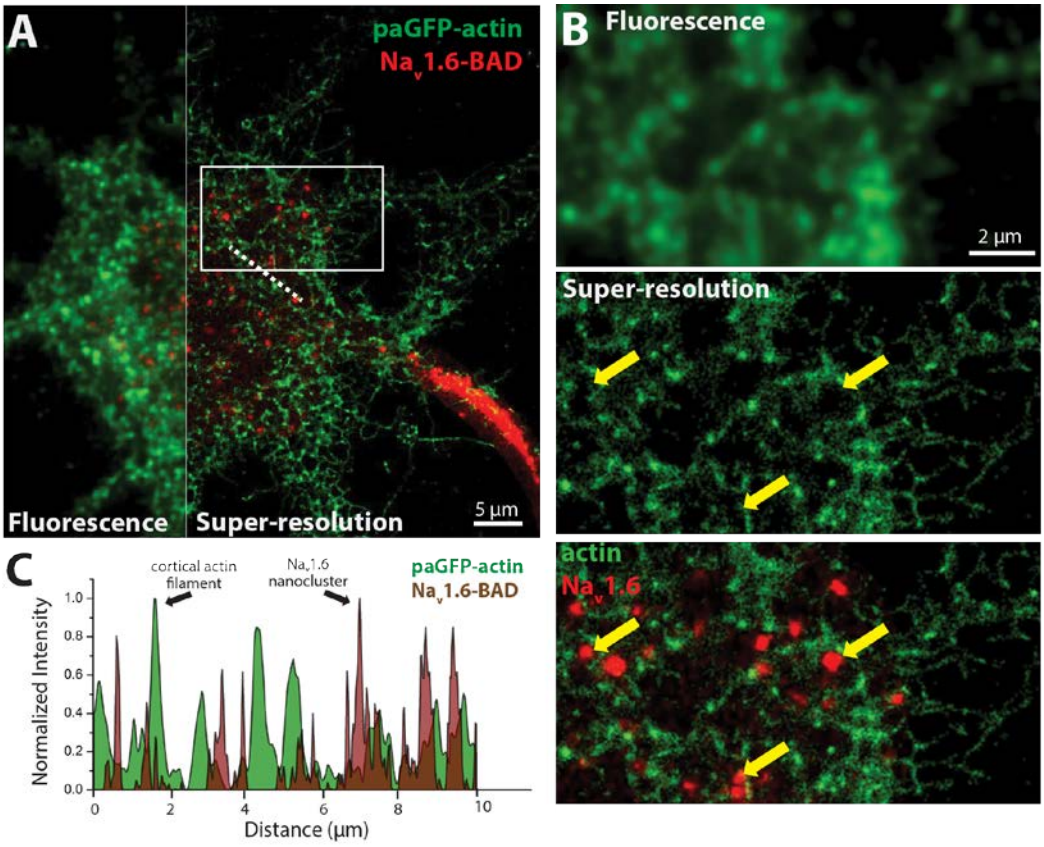


**SUPPLEMENTARY FIGURE 2 $Na_v1.6$ nanoclusters are not associated with cortical actin.** (A) DIV10 rat hippocampal neuron transfected with photoactivatable-GFP-actin (paGFP-actin) and $Na_v1.6$-BAD. Surface distribution of $Na_v1.6$ visualized with CF640R. PALM-based super-resolution image of paGFP-actin (right side) was reconstructed from cycles of activation and photobleaching of individual paGFP-tagged actin molecules. The super-resolution image reveals fine actin structures not visible with light microscopy (left side). The single process with dense CF640 surface labeling is the axon initial segment. (B) Enlargement of white box in (A) showing the diffraction limited TIRF image of cortical actin (top panel), the paGFP-actin PALM reconstruction (middle panel) and an overlay of the $Na_v1.6$-BAD surface nanoclusters, visualized with CF640, with the paGFP-actin PALM reconstruction (bottom panel). (C) Line scan showing the normalized fluorescence intensity of actin (green) or $Na_v1.6$ (dark red) of the dotted white line in (A). $Na_v1.6$ nanoclusters (yellow arrows) are generally adjacent to, but not co-localized with cortical actin filaments.

To further address whether actin is involved in $Na_v1.6$ localization to nanoclusters, we imaged the distribution of $Na_v1.6$-BAD in the presence of 200 nM swinholideA (swinA), a drug that induces both f-actin depolymerization and depletion of G-actin. Fig. S3 shows a neuron

expressing $Na_v1.6$-BAD and Ruby-Lifeact, a fluorescent f-actin-binding peptide (3). The neuron was imaged in TIRF with a slow frame rate (once per min) to minimize photobleaching, and swinA was added after 10 min of imaging to establish a baseline. Fig. S3, top panels, show the imaging of Ruby-Lifeact and cell surface $Na_v1.6$-BAD following swinA addition. The change in Ruby-Lifeact fluorescence confirmed swinA-induced f-actin depolymerization. The bottom panels show an enlargement of the area denoted by the white box that contains three nanoclusters (yellow arrows) present before the addition of swinA. The location of the clusters remains remarkably consistent for 75 min after the addition of swinA.

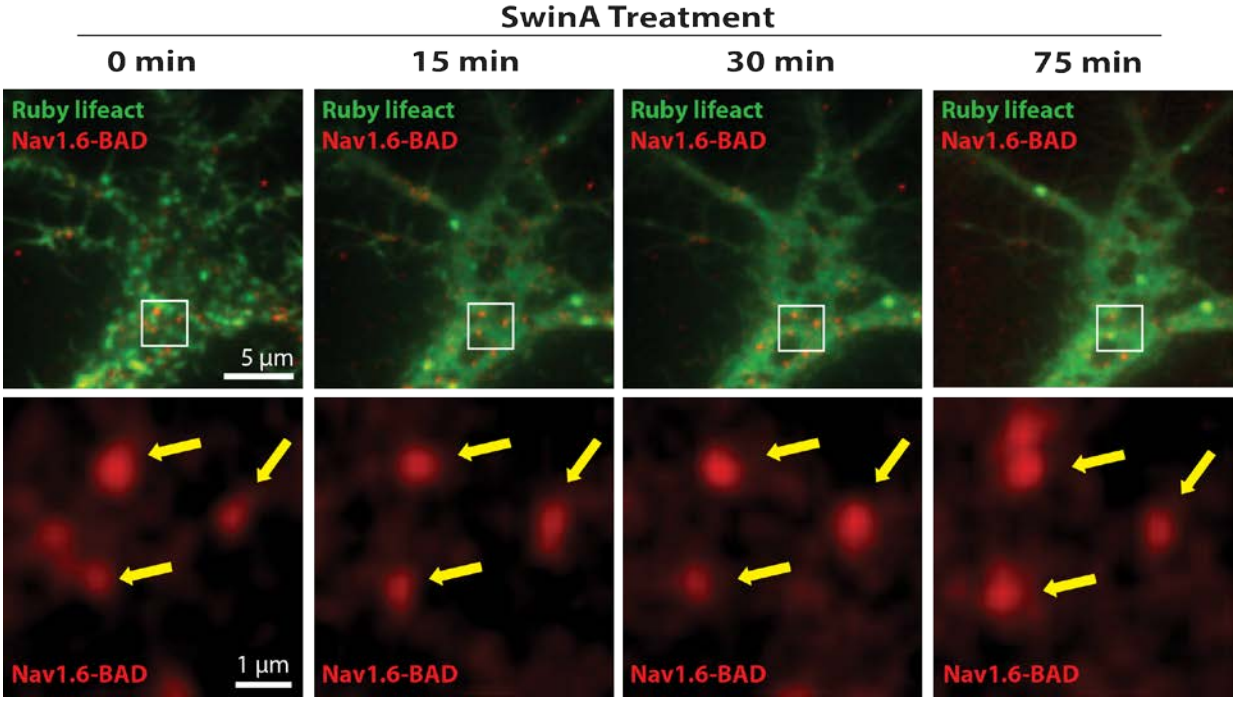


**SUPPLEMENTARY FIGURE 3 Actin depolymerization does not dissolve $Na_v1.6$ nanoclusters.** A neuron expressing $Na_v1.6$-BAD and Ruby-Lifeact was imaged in TIRF. $Na_v1.6$-BAD was labeled with CF640 to visualize the surface distribution. The top panels illustrate the Ruby-Lifeact and $Na_v1.6$ nanocluster fluorescence in the presence of 200 nM swinA. The bottom panels show enlargements of the respective white boxes shown above, each containing three stable $Na_v1.6$ nanoclusters. Images were acquired once every min. The fluorescence intensity and location of the nanoclusters remained constant for more than 1 hour after actin depolymerization (yellow arrows). Ruby-Lifeact labeled actin filaments were used to demonstrate the effectiveness of swinA treatment.

**$Na_v1.6$ nanoclusters do not colocalize with clathrin-coated pits, mitochondria or $K_v2.1$ induced ER-plasma membrane junctions**

We next investigated colocalization of the $Na_v1.6$ nanoclusters with several scaffold/organelle markers. We first imaged clathrin-light-chain tagged with GFP (CLC-GFP) to determine whether the $Na_v1.6$ nanoclusters were formed via channel localization to endocytic sites (Fig. S4A). However, the surface $Na_v1.6$-BAD channels labeled with SA-CF640 did not co-localize with CLC-GFP. This result indicates that the nanoclusters are not endocytic platforms. This is consistent with the long lifetime seen for the nanoclusters since clathrin-coated pits tend to be transient (seconds to minutes) (4, 5). This does not exclude, however, that small numbers of $Na_v1.6$ channels could interact with clathrin since all proteins have a basal rate of protein turnover. Mitochondria localize near membrane-bound proteins and regulate them through calcium and oxidative signaling (6). Therefore, MitoTracker was used to identify mitochondria in live neurons and SA-488 was used to label the surface $Na_v1.6$-BAD. Mitochondria close to the plasma membrane were imaged in TIRF and compared to the distribution of $Na_v1.6$. No apparent relationship between mitochondria and the somatic nanoclusters was observed (Fig. S4B).

We next looked at the distribution of the $Na_v1.6$ nanoclusters in relation to the delayed rectifier $K_v$ channel, $K_v2.1$, which forms large micron-sized clusters on the soma and AIS of some neurons (7, 8). These channels were recently found to mediate the formation of junctions between the endoplasmic reticulum and plasma membrane (ER-PM junctions), which act as membrane trafficking hubs (9). We co-expressed $Na_v1.6$-BAD and GFP-$K_v2.1$, labeling surface $Na_v1.6$ with SA-594. $Na_v1.6$ nanoclusters were found around, but not within, large $K_v2.1$ clusters, as seen in Fig. S4C. This exclusion from $K_v2.1$-induced ER-PM junctions is likely due

to the large intracellular mass of the $Na_v1.6$ channel and may explain regions of soma membrane that were consistently devoid of $Na_v1.6$ single molecule tracks.

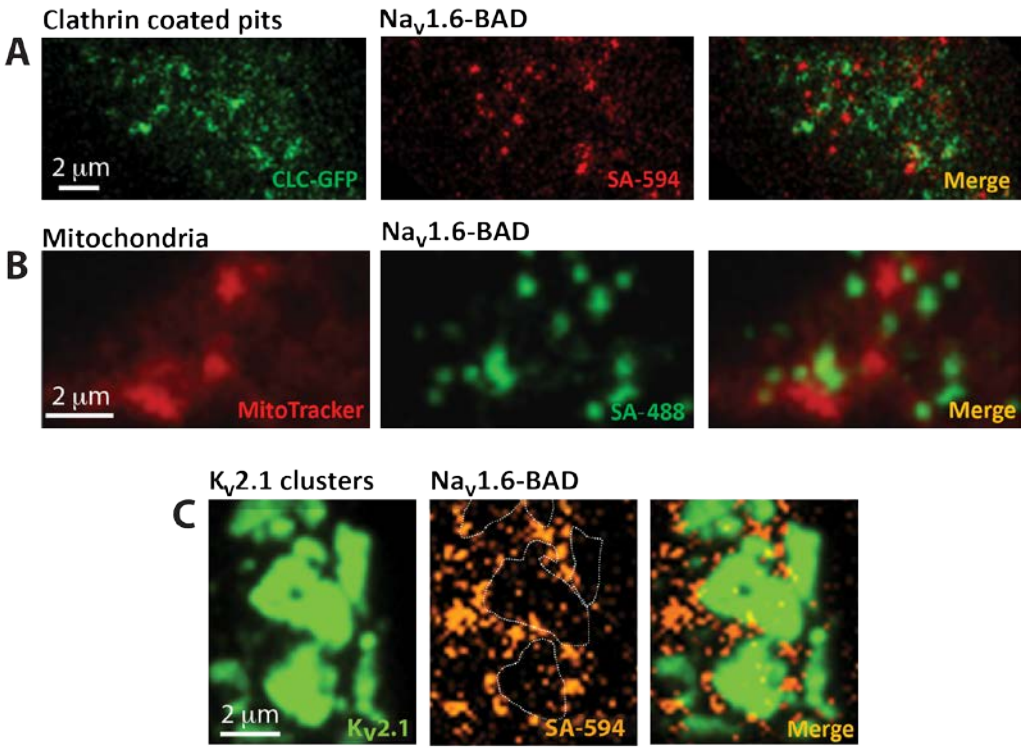


**SUPPLEMENTARY FIGURE 4 $Na_v1.6$ clusters do not co-localize with endocytic sites, mitochondria or ER-PM junctions.** (A) Neurons transfected with GFP-clathrin-light-chain (left green panel) and $Na_v1.6$-BAD labeled with SA-594 (red middle panel) show no significant co-localization as observed on the merge panel (right). (B) Mitochondria were labeled with MitoTracker (left panel, red) in live neurons transfected with $Na_v1.6$-BAD that was surface labeled in this case with SA-488 (middle panel, green). No apparent co-localization was observed. (C) Neurons co-transfected with GFP-$K_v2.1$, a marker of ER-PM junctions, (green) and $Na_v1.6$-BAD surface labeled with SA-594 (orange). The merged image of the two channels (right panel) shows how GFP-$K_v2.1$ (green) and $Na_v1.6$-BAD-SA594 (orange) localize to mutually exclusive regions, with $Na_v1.6$ nanoclusters located outside of the $K_v2.1$ clusters, and only few single channels located inside. All panels correspond to a somatic region of a neuron imaged in TIRF.

## SUPPORTING REFERENCES


1. Ovesný, M., P. Křížek, J. Borkovec, Z. Švindrych, and G. M. Hagen. 2014. ThunderSTORM: a comprehensive ImageJ plug-in for PALM and STORM data analysis and super-resolution imaging. Bioinform. 30:2389-2390.
2. O'Connell, K. M., A. S. Rolig, J. D. Whitesell, and M. M. Tamkun. 2006. Kv2.1 potassium channels are retained within dynamic cell surface microdomains that are defined by a perimeter fence. J. Neurosci. 26:9609-9618.
3. Riedl, J., A. H. Crevenna, K. Kessenbrock, J. H. Yu, D. Neukirchen, M. Bista, F. Bradke, D. Jenne, T. A. Holak, and Z. Werb. 2008. Lifeact: a versatile marker to visualize F-actin. Nat. Methods 5:605-607.
4. Weigel, A. V., M. M. Tamkun, and D. Krapf. 2013. Quantifying the dynamic interactions between a clathrin-coated pit and cargo molecules. Proc. Natl. Acad. Sci. USA. 110:E4591-E4600.
5. Loerke, D., M. Mettlen, D. Yarar, K. Jaqaman, H. Jaqaman, G. Danuser, and S. L. Schmid. 2009. Cargo and dynamin regulate clathrin-coated pit maturation. PLoS Biology 7:e1000057.
6. Chaplin, N. L., M. Nieves-Cintrón, A. M. Fresquez, M. F. Navedo, and G. C. Amberg. 2015. Arterial smooth muscle mitochondria amplify hydrogen peroxide microdomains functionally coupled to L-type calcium channels. Circ. Res. 117:1013-1023.
7. Sarmiere, P. D., C. M. Weigle, and M. M. Tamkun. 2008. The $K_v2.1$ $K^+$ channel targets to the axon initial segment of hippocampal and cortical neurons in culture and in situ. BMC Neurosci. 9:112.
8. Tamkun, M. M., K. M. O'Connell, and A. S. Rolig. 2007. A cytoskeletal-based perimeter fence selectively corrals a sub-population of cell surface Kv2.1 channels. J. Cell Sci. 120:2413-2423.
9. Fox, P. D., C. J. Haberkorn, E. J. Akin, P. J. Seel, D. Krapf, and M. M. Tamkun. 2015. Induction of stable endoplasmic reticulum/plasma membrane junctions by $K_v2.1$ potassium channels. J. Cell Sci. 128:2096-2105.


## MOVIE LEGENDS

**MOVIE S1. Diffusion behavior of Nav1.6 channels on the somatic surface.** Surface channels were labeled with SA-CF640R and imaged at 10 Hz using TIRF microscopy. The yellow arrows point to static nanoclusters while the white arrow points to a region that transiently accumulates individual channels.

**MOVIE S2. Diffusion behavior of Nav1.6 channels on the glial cell surface.** Surface channels labeled with SA-CF640R were imaged at 10 Hz using TIRF microscopy.